Effect of MgAl-layered double hydroxide exchanged with linear alkyl carboxylates on fire-retardancy of PMMA and PS†

Calistor Nyambo,[a] Ponusa Songtipya,[bc] E. Manias,[b] Maria M. Jimenez-Gasco[c] and Charles A. Wilkie*[a]

Received 17th April 2008, Accepted 1st July 2008
First published as an Advance Article on the web 4th August 2008
DOI: 10.1039/b806531d

Alkyl carboxylate-modified layered double hydroxides (LDH) were prepared and used as nanofillers for poly(methyl methacrylate) (PMMA) and polystyrene (PS). The LDH intercalated with long-chain linear alkyl carboxylates ($CH_3(CH_2)_nCOO^-$, $n = 8$, 10, 12, 14, 16, 20) were prepared *via* anionic exchange of MgAl–nitrate, showing a systematic increase in basal spacing with longer alkyls. MgAl–undecenoate LDH was prepared by co-precipitation. The MgAl–LDHs were melt blended with poly(methyl methacrylate) and bulk polymerized with styrene to form nanocomposites. The dispersion of the MgAl–LDH in the polymers was investigated by transmission electron microscopy and X-ray diffraction. Thermal and fire properties were studied using cone calorimetry and thermogravimetric analysis; the thermal stability of both polymers was enhanced and a very significant reduction in the peak heat release rate was observed for almost all of the poly(methyl methacrylate) composites and a few of the polystyrene composites.

1. Introduction

The use of layered double hydroxides, LDHs, to form polymer–clay (nano)composites and their potential usage as fire-retardant additives is of increasing interest.[1,2] LDHs, also known as hydrotalcite-like materials, are anionic clays that are inexpensive to prepare and are environmentally friendly.[3]

Hydrotalcite-like compounds, LDHs, have the general formula $[M^{2+}_{1-x}M^{3+}_x(OH)_2][A^{n-}_{x/n}]\cdot mH_2O$ where M^{2+} is a divalent cation (*e.g.* Mg^{2+}) and M^{3+} a trivalent cation (*e.g.* Al^{3+}), while A^{n-} is a charge-balancing interlayer anion.[4] The Mg–O–Al–OH layer is positively charged, and electrical neutrality is achieved by the presence of hydrated exchangeable anions in the interlamellar space, such as nitrate.[5] These interlayer anions can be exchanged, for example with anionic surfactants such as carboxylates,[6] sulfonates,[7] or phosphonates,[8] providing an effective method for incorporating various functionalities and tunable surface properties on the LDH. Hydrotalcites are commercially available from several sources but these materials usually contain carbonate impurities. If one wishes to vary either the stoichiometry, divalent or trivalent metals or the anion, it is necessary to make these in the laboratory.

In this work, for example, we synthesized LDHs based on Mg and Al, designed to resemble commonly used fire-retardant additives, *cf.* magnesium hydroxide (MDH) and alumina trihydrate (ATH) and these LDHs are compared to the simple minerals. Subsequent incorporation of linear-chain alkyl carboxylates [$CH_3(CH_2)_nCOO^-$ with $n = 8$, 10, 12, 14, 16, 20 and 10-undecenoate] between the layers of the MgAl–LDH was used to systematically vary their properties; the effect of the alkyl chain length on morphology, thermal stability, mechanical and fire properties was studied. In previous work from these laboratories, we have investigated the dependence on the divalent metal in an LDH. A magnesium–aluminium LDH is reasonable well-dispersed in poly(methyl methacrylate) PMMA, and shows enhanced thermal stability by TGA and a significant reduction in the peak heat release rate (PHRR) in the cone calorimeter.[9] Zinc, cobalt, nickel and copper have also been used. Cobalt exhibits the best dispersion in PMMA and the largest reduction in the peak heat release rate. The ZnAl LDH system also shows significant reduction in PHRR.[10]

These organically modified LDHs can be readily used as nanofillers or additives for common polymers, yielding varied dispersions depending on the polymer matrix. Here we explore poly(methyl methacrylate) (PMMA) and polystyrene (PS), as representatives of polar and non-polar polymers. The effect of the synthesized organo-LDHs on the fire and thermal properties of PS and PMMA was studied, and compared with composites with commercially available additives (MDH, ATH, and MDH–ATH mixtures).

2. Experimental

2.1 Materials

The materials used in the synthesis of magnesium layered double hydroxides were $Mg(NO_3)_2\cdot 6H_2O$ (Aldrich Chemical Co.), $Al(NO_3)_3\cdot 9H_2O$ (Aldrich Chemical Co.), NaOH (Aldrich Chemical Co.), palmitic acid 95% (TCI), methanol (Alfa Aesar), benzoyl peroxide (Aldrich Chemical Co.), styrene monomer (Aldrich Chemical Co.), behenic acid 80% (TCI), decanoic acid (98%) (Aldrich Chemical Co.), stearic acid (95%) (Avocado Research Chemicals), lauric acid (Eastman), myristic acid (95%) (Acros Chemicals). Commercial polymers poly(methyl

[a]*Department of Chemistry, Marquette University, Milwaukee, WI 53201-1881, USA*
[b]*Department of Materials Science and Engineering, Penn State University, University Park, PA, USA*
[c]*Plant Pathology Department, Penn State University, University Park, PA, USA*

† Electronic supplementary information (ESI) available: Fig. S1–S11 and Table S1. See DOI: 10.1039/b806531d

methacrylate) (PMMA, M_w120 000) and polystyrene (PS, $M_w \sim 230\,000$, $M_n \sim 140\,000$, softening point 107 °C Vicat, ASTM D1525 melt index 7.5 g per 10 minutes) were purchased from the Aldrich Chemical Co. Magnesium hydroxide (MDH) (magnifin H7-C) and alumina trihydrate (ATH) (martinal char 42) were supplied by Albemarle Corp. All chemicals were used without further purification.

2.2 Preparation of magnesium aluminium nitrate LDH (MgAl–NO_3 LDH)

The magnesium aluminium nitrate layered double hydroxide (MgAl–NO_3 LDH) was synthesized by the co-precipitation method, following a procedure similar to that reported by Meyn *et al.*[11] The preparation was performed under a nitrogen atmosphere to exclude carbonate from the LDHs. A solution of 32.0 g of $Mg(NO_3)_2 \cdot 6H_2O$ (0.125 mol) and 23.4 g of $Al(NO_3)_3 \cdot 9H_2O$ (0.0625 mol) in 125 ml of degassed and deionized water was added dropwise over 1 hour to a solution of 12.5 g of NaOH (0.313 mol) and 18.2 g of $NaNO_3$ (0.214 mol) in 145 ml of degassed/deionized water. The pH of the solution was maintained at 10.0 by adding 1M NaOH solution, as needed. The resulting white precipitate was aged for 24 hours at 65 °C, then filtered until all of the supernatant liquid was removed. The sample was washed several times with large amounts of deionized and degassed water, and was dried at 50 °C in a vacuum oven.

2.3 Preparation of alkyl carboxylate-exchanged magnesium aluminium LDHs (MgAl–C*n*)

Intercalation of linear alkyl anions in the MgAl–LDHs was done through ion-exchange reactions. Specifically, alkyl carboxylates, *i.e.*, decanoate ($C_{10}H_{19}O_2^-$ or C10), laurate (C12), myristate (C14), palmitate (C16) and stearate (C18) were used to exchange the NO_3^- ions in the MgAl–NO_3 LDH. In a typical preparation, 5 g of the MgAl–NO_3 LDH were dispersed in 100 ml of an 0.008 M anion solution prepared by dissolving the organic acid in a warm water–methanol solution (1 : 1 volume ratio) containing 0.008 M of NaOH under a steady flow of nitrogen to exclude carbon dioxide. The solution was vigorously stirred for 24 hours at 50 °C and the solid was separated, washed with degassed/de-ionized water and dried at 40 °C. For the behenate (C22), a 0.004 M solution was used for the exchange reaction. All the exchange reactions of the MgAl–LDHs was repeated several times and completion of exchange was ascertained by the absence of the 1384 cm^{-1} NO_3^- band in the IR spectra of all of the MgAl–LDHs.

2.4 Preparation of the MgAl–undecenoate LDH (MgAl–C11)

The magnesium aluminium undecenoate layered double hydroxide (MgAl–C11) was prepared following a literature procedure.[12] A solution of $Mg(NO_3)_2 \cdot 6H_2O$ (0.02 mol) and $Al(NO_3)_3 \cdot 6H_2O$ (0.01 mol) in deionized and decarbonated water (50ml) was added dropwise to a solution of 10-undecenoic acid (0.02 mol) and NaOH (0.02 mol) in deionized and decarbonated water (100 ml) with vigorous mixing under an inert nitrogen atmosphere. The pH was maintained at 10.0 by adding 1M NaOH solution. The resultant slurry was aged at 60 °C for 24 hours, cooled to room temperature, and repeatedly washed with deionized and decarbonated water before drying under an inert atmosphere at a temperature of 50 °C.

Table 1 Composition of the melt-blended composites based on commercial MDH and ATH additives. Both PS- and PMMA-based composites were prepared by the following compositions. All compositions are % by weight

Formulation	% Polymer	% MDH	% ATH
Pure (unfilled polymer)	100	0	0
+ 3% MDH	97	3	0
+ 5% MDH	95	5	0
+ 10% MDH	90	10	0
+ 20% MDH	80	20	0
+ 3% ATH	97	0	3
+ 5% ATH	95	0	5
+ 10% ATH	90	0	10
+ 20% ATH	80	0	20
+ 2% MDH + 1% ATH	97	2	1
+ 3.3% MDH + 1.7% ATH	95	3.3	1.7
+ 6.7% MDH + 3.3% ATH	90	6.7	3.3

2.5 Preparation of the polymer composites

PMMA nanocomposites were prepared by melt blending, using a Brabender Plasticorder, at a temperature of 180 °C, screw speed of 60 rpm and residence time of 7 min. The nanocomposites were prepared at loadings of 3, 5 or 10 wt% of each exchanged MgAl–LDH. A reference sample of pure (unfilled) PMMA was also prepared using the same procedure. Melt-blended polystyrene and PMMA composites containing MDH and ATH were also prepared using the same procedure; containing 3 to 20 wt% of MDH or ATH, or 3 to 10 wt% of a 2 : 1 MDH–ATH mixture (the formulations are summarized in Table 1).

Polystyrene composites containing alkyl-exchanged MgAl–LDHs were prepared *via* bulk polymerization of styrene monomer (99%) using a known procedure.[13] The styrene monomer was first passed through a column packed with inhibitor remover for *t*-butylcatechol; subsequently, 3, 5 or 10 wt% of exchanged MgAl–LDH was dispersed in the monomer for 24 hours, followed by the addition of 1% benzoyl peroxide initiator. The mixture was heated to 70 °C for 24 hours. The PS was recovered, ground, and dried in a vacuum oven at 90 °C for 24 hours. Virgin (unfilled) styrene polymer was prepared using same procedure, without the MgAl–LDH.

3. Results and discussion

3.1 Elemental analysis

Elemental analysis was carried out by inductively coupled plasma at Huffman Laboratories in Colorado. Table 2 summarizes the results and the corresponding formulae of the LDHs. The anion-exchange capacities, AEC, of the MgAl–LDHs are also included in Table 2. These are higher than the cation-exchange capacities, CEC, of typical montmorillonites (MMT)[14] and decrease as the chain length of carboxylate anion increases in the LDH, consistent with the definition that includes the molar mass of the LDH.[15] The Mg^{2+}/Al^{3+} molar ratios in the LDHs correlate perfectly with the amounts used during preparation, and are consistent with ratio values reported in the literature.[15]

Table 2 Chemical formulae, AEC and Mg : Al mole ratio of the synthesized LDH

LDH	Analytically determined composition	[a]AEC/mequiv per 100 g	Mole ratio Mg : Al
MgAl–Nitrate	$Mg_{0.65}Al_{0.36}(OH)_2(NO_3^-)_{0.35}(CO_3)_{0.01}\cdot 0.51\ H_2O$	287	1.81
MgAl–C10	$Mg_{0.67}Al_{0.33}(OH)_2(C_{10}H_{19}O_2)_{0.17}(C_{10}H_{19}O_2Na)_{0.01}(NO_3)_{0.01}(CO_3)_{0.05}\cdot 0.42\ H_2O$	326	2.07
MgAl–C11	$Mg_{0.67}Al_{0.33}(OH)_2(C_{11}H_{19}O_2)_{0.31}(NO_3)_{0.02}\cdot 0.42\ H_2O$	263	2.03
MgAl–C12	$Mg_{0.66}Al_{0.34}(OH)_2(C_{10}H_{31}O_3)_{0.30}\cdot(CO_3)_{0.02}.\ 0.43\ H_2O$	266	1.95
MgAl–C14	$Mg_{0.67}Al_{0.33}(OH)_2(C_{14}H_{27}O_2)_{0.33}\cdot 0.51\ H_2O$	230	2.07
MgAl–C16	$Mg_{0.67}Al_{0.33}(OH)_2(C_{16}H_{31}O_2)_{0.33}\cdot 0.69\ H_2O$	211	2.03
MgAl–C18	$Mg_{0.68}Al_{0.32}(OH)_2(C_{18}H_{35}O_2)_{0.32}\cdot 0.36\ H_2O$	201	2.11
MgAl–C22	$Mg_{0.68}Al_{0.32}(OH)_2(C_{22}H_{43}O_2)_{0.32}\cdot 0.40\ H_2O$	183	2.08

[a] The anion-exchange capacity, AEC, is calculated as follows: $AEC = x/M_w \times 10^5$ (mequiv per 100 g) where M_w is the weight of the chemical formula for each octahedral unit. x is the stoichiometric value of the trivalent cation in the chemical formula for each octahedral unit.

3.2 Infrared spectroscopy FT-IR

Fig. 1 shows the IR spectra of the alkyl carboxylate-exchanged MgAl–LDHs obtained from the MgAl–nitrate LDH, and the MgAl–C11 prepared from co-precipitation. The absence of the NO_3^- bands at 1384 cm^{-1} in the spectra of all of the exchanged LDHs indicates that the exchange process was complete. The MgAl–C10 and MgAl–C12 LDHs showed two small peaks at 1365 cm^{-1}, due to some carbonate impurity. This is a common problem with most methods of preparing LDHs, including the co-precipitation method, since contamination with carbon dioxide typically result in the formation of a carbonate anion that is readily incorporated and tenaciously held in the interlayer (*cf.* Table 2).[16,17] This minor contamination may have occurred during sample transfer, even though decarbonated and deionized water was used and exposure to the atmosphere was kept to a minimum. The observations from infrared spectroscopy for all the LDHs are similar, as shown Fig. 1. The bands are observed at 3408 cm^{-1}, corresponding to the OH vibration; at 2922 and 2852 cm^{-1}, due to C–H stretch; at 1636 cm^{-1}, due to OH vibration of water molecules; at 1557 and 1468 cm^{-1}, characteristic of the asymmetric- and symmetric-stretching vibration of the $RCOO^-$; these last peaks, and the absence of the nitrate band, confirm the presence of the linear alkyl carboxylate in the galleries of the LDH. The IR spectra of the MgAl–C11 shows a small peak at 1642 cm^{-1}, which is characteristic of the C=C stretching vibration of the 10-undecenoate anion.

3.3 Powder XRD for the exchanged MgAl–LDHs

The anion exchange of the magnesium aluminium nitrate layered double hydroxide (MgAl–NO_3 LDH) was confirmed by powder X-ray diffraction. Fig. 2 shows the XRD patterns for all the organically modified LDHs obtained from the MgAl–NO_3 LDH and the MgAl–C11 obtained from co-precipitation. After exchange of all the nitrate anions, the d_{003} peak of the MgAl–NO_3 LDH shifts to lower 2θ angles from that of MgAl–NO_3 ($2\theta = 9.98\ ^\circ$) indicating an increase in the gallery height as the nitrate is exchanged by the much larger alkyl carboxylate. In addition, all the XRD patterns for the exchanged LDHs show higher order 003n diffraction peaks, indicating good layering in the intercalated structures, *i.e.*, a long coherence length in the 003 stacking direction denoting high numbers of parallel-aligned alkyl-exchanged LDH layers.

Fig. 2 also shows the XRD data for the carboxylate exchanged MgAl–LDH, from the nitrate form. The Bragg d-spacings for the interlayer distance, d_{003}, show an increasing trend with the length of the alkyl. A plot of the d-spacing *versus* the number of carbons

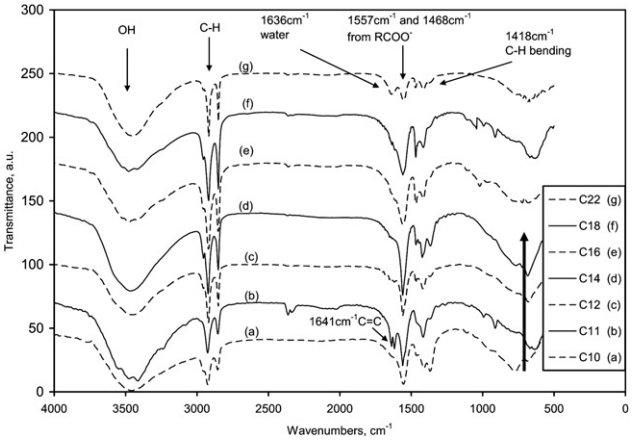

Fig. 1 Overlay of FT-IR spectra for (a) MgAl–C10, (b) MgAl–C11, (c) MgAl–C12, (d) MgAl–C14, (e) MgAl–C16, (f) MgAl–C18 and (g) MgAl–C22 LDHs.

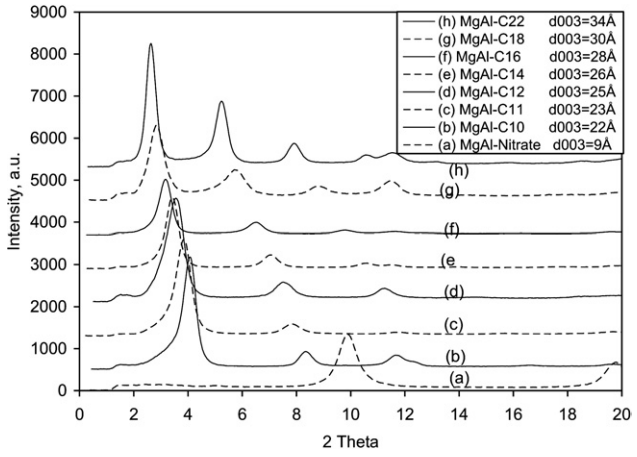

Fig. 2 XRD traces for (a) MgAl–NO_3^-, (b) MgAl–C10, (c) MgAl–C11, (d) MgAl–C12, (e) MgAl–C14, (f) MgAl–C16, (g) MgAl–C18 and (h) Mg1Al–C22 LDHs.

in the surfactant is shown in the ESI†; indicating a linear correlation between the number of carbons in the alkyl carboxylate and the *d*-spacing of the exchanged LDH. This is characteristic of high ion-exchange capacity layered materials when exchanged at capacity by long alkyls.[18] Miyata and Kimura also reported a similar linear increase in *d*-spacing with the number of carbon atoms of dicarboxylates in $Zn^{2+}Al^{3+}$–LDHs.[19]

XRD data may also show the presence of extended impurity phases, such as carbonate, in the LDH.[17] For example, if the carbonate exists as a separate layered phase, a Bragg diffraction peak normally appears at $2\theta = 11.6$ °, corresponding to the *d*-spacing of 7.80 Å of the MgAl–carbonate LDH. As shown by XRD, such a carbonate phase is absent in all the XRD traces, including those of MgAl–C10 and MgAl–C12 LDHs, which showed carbonate peaks in IR. The IR detects the presence of carbonate but, given its very low concentration as indicated by the elemental analyses (Table 2), it is not expected to form an extended carbonate interlayer phase that would give rise to a basal diffraction.

3.4 Morphology of the PMMA + MgAl–LDHs composites

To a first approximation, the nanocomposite structure can be characterized by monitoring the XRD pattern (position, shape and intensity of the XRD peaks, or lack thereof, background intensity, *etc.*). Plots of XRD patterns for all the composites are shown in the ESI†. For PMMA + 3% MgAl–C10 the 003 diffraction peaks of the MgAl–LDH disappeared, suggesting exfoliation. For all other composites, the 003 diffraction peaks shift to lower values of 2θ and reduce in intensity; for the PMMA composites 3% MgAl–C12, MgAl–C14, MgAl–C16, MgAl–C18 and MgAl–C22, the respective d_{003} increases by 9.1 Å, 11.0 Å, 12.3 Å, 11.5 Å and 11.5 Å compared to the respective alkyl-exchanged LDH. These increases in *d*-spacing indicate expansion of the LDH layers due to intercalation of the polymer, and are consistent with the creation of a bilayer –two monomers wide – polymer structure in the gallery.[20,23] Second order 006 diffraction peaks were observed in the composites with LDHs containing longer alkyl chains *i.e.* PMMA + 3% MgAl–C18 and PMMA + 3% MgAl–C22.

Further characterization of the nanocomposite structure was obtained from direct observation of the LDH dispersion *via* bright-field transmission electron microscopy (TEM). Typical TEM images for some of the PMMA_LDH systems (C10, C16 and C18) are shown in Fig. 3 and TEM images from the remaining systems have been included in the ESI†. XRD suggests exfoliation for PMMA + 3% MgAl–C10. This suggestion was confirmed by the TEM, as shown in Fig. 3. The MgAl–C10 layers are mostly isolated and uniformly dispersed in PMMA at low magnification. There may also been some small tactoids present. At higher magnification, the MgAl–C10 layers are not parallel, which is in concert with the absence of a 003 basal reflection in the XRD trace. XRD data also suggests intercalation in MgAl–C12, MgAl–C14, MgAl–C16, MgAl–C18 and MgAl–C22 PMMA nanocomposites, which is also confirmed by TEM observation. All of the carboxylates larger than C10 show evidence of intercalation and, in many instances, *e.g.*, C12, C14 and C16, show clay layers both in and out of registry, *i.e.*, both intercalated and exfoliated. For C18 and C22, only layers in parallel registry can be seen. The best descriptions of the nanocomposite morphology are: C10, exfoliated; C12, C14, C16, mixed intercalated–exfoliated; C18 and C22, intercalated.

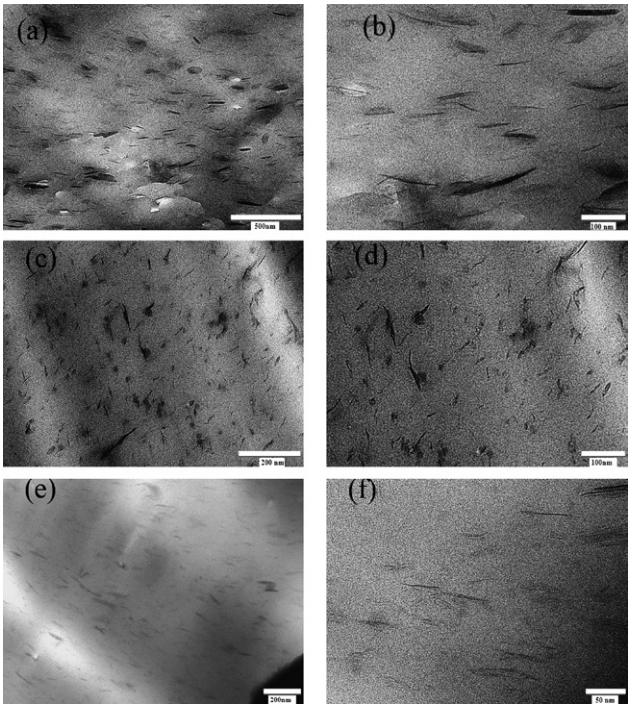

Fig. 3 TEM images at (a) low and (b) high magnification for PMMA + 3% MgAl–C10, (c) low and (d) high magnification for PMMA + 3% MgAl–C16, and (e) low and (f) high magnification for PMMA + 3% MgAl–C18. The scale bars are indicated on the images.

3.5 Morphology of the PS + MgAl–LDHs composites

The XRD traces for the PS + MgAl–LDHs composites, all prepared by bulk polymerization, are shown in the ESI†. In general, there is at best only a small shift of the 003 peaks to lower 2θ values. The low intensity and the breadth of these peaks make it difficult to assign peak maxima and thus to arrive at an accurate *d*-spacing for the composites; our best fits place the composite d_{003}-spacings at just 3 to 5 Å above those of the respective alkyl-modified LDHs, an interlayer gallery expansion that is barely enough to accommodate even a monolayer – one monomer wide – of polystyrene[21–23] The XRD traces for C14, C18 and C22 composites show no 003 peak but, based upon the lower homologues, this is likely due to disordered LDH layers in mostly immiscible nanocomposites (microcomposites), rather than an indication of a well exfoliated nanocomposite structure.

For the PS composites a direct observation of the LDH dispersion with TEM seems highly necessary. The TEM images for the PS + MgAl–C11 LDH composite are presented in Fig. 4, while the structure of the C22 composite is shown in Fig. 5; TEM images for the remaining PS–LDH composites (C10 to C18) are given in the ESI†. The PS/MgAl–C11 composites show a qualitatively different dispersion than the PS composites based on

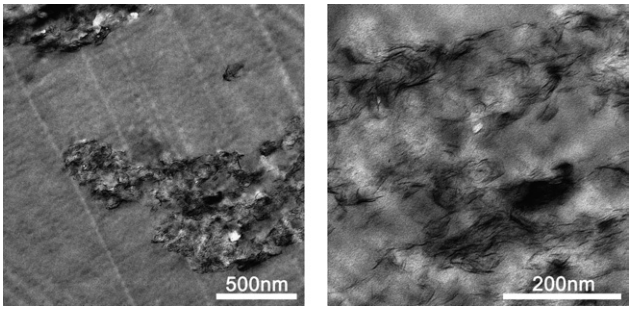

Fig. 4 The structure of the PS composite reinforced by the 10-undecenoic acid modified MgAl (*cf.* MgAl–C11), by bright-field TEM imaging.

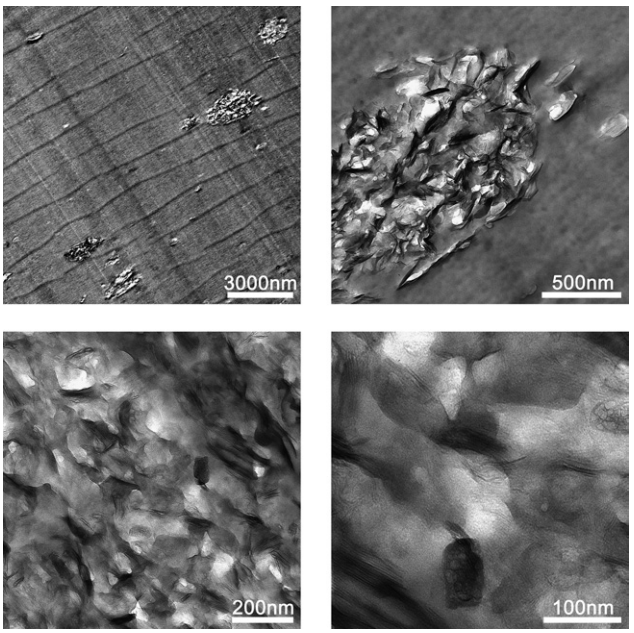

Fig. 5 Hierarchical structure of the PS composites with linear alkyl carboxylate (C10–C20)-modified MgAl, as exemplified by bright-field TEM imaging of the structure of MgAl–C22 at various magnifications.

alkyl carboxylate (C10–C22) modified MgAl. Specifically, at the micrometre scale, the MgAl–C11 shows a substantially better swelling of the agglomerates by PS, with most of the tactoids being delaminated down to individual layers or highly-disordered well-dispersed groups of a few layers (nanometre scale). Very few tactoids, typically composed of the larger lateral-dimension LDH layers, retain their parallel registry (intercalated tactoid structures). This carboxylate contains a terminal double bond, which may have participated in the polymerization and thus could have led to better LDH nano-dispersion. This has also been seen with MMT systems.[24] For the composites based on saturated alkyl-exchanged MgAl LDHs (Fig. 5), the dispersion at the nano-scale level is similar to PS/montmorillonite systems.[21,22] At the micrometre scale, the MgAl LDHs show definitive agglomeration (moderate to poor dispersions) characteristic of the "conventional composite"/microcomposite structures of typical polystyrene/LDH composites. However, they show good dispersions at the nanoscale, with individual LDH layers being separated by polystyrene, forming intercalated or disorderly swollen tactoids of LDH layers (Fig. 5 and ESI†). The extent/tendency of PS intercalation between the organically modified LDH seems to be increasing with longer alkyl lengths of the carboxylates, in concert with the X-ray diffraction data for the 003 LDH reflection, as might be expected since the gallery space becomes more organophilic and thus more compatible with the polymer. This dispersion improvement with the length of the alkyl-anion in the LDH, is also reflected in better swelling of the agglomerates by PS at the micrometre scale, however all the composites can be assigned as microcomposites, and only for the PS + MgAl–C22 was the presence of a few isolated/exfoliated LDH layers in the polymer observed.

3.7 Thermal stability of the MgAl–LDHs and their composites

Fig. 6 shows the thermogravimetric analysis (TGA, carried out under a N_2 flow) and the associated data of the alkyl carboxylate-exchanged MgAl–LDHs. The thermal stability can be quantified through the onset temperature of degradation, usually associated with the temperature at 10% mass loss, $T_{0.1}$,

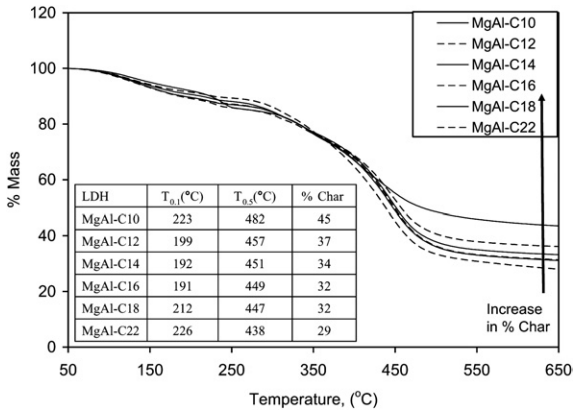

LDH	$T_{0.1}$(°C)	$T_{0.5}$(°C)	% Char
MgAl-C10	223	482	45
MgAl-C12	199	457	37
MgAl-C14	192	451	34
MgAl-C16	191	449	32
MgAl-C18	212	447	32
MgAl-C22	226	438	29

Fig. 6 TGA of the MgAl–LDHs.

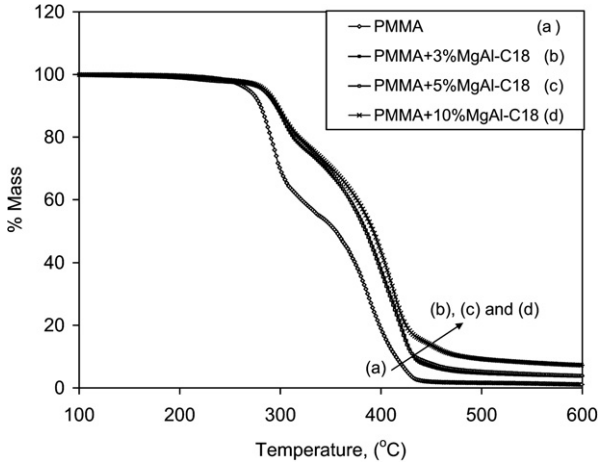

Fig. 7 TGA results for (a) PMMA, (b) PMMA + 3% MgAl–C18, (c) PMMA + 5% MgAl–C18 and (d) PMMA + 10% MgAl–C18.

the mid-point of the degradation, $T_{0.5}$, and the fraction of residue that remains at the end of the run. All alkyl-exchanged LDHs were dried at 50 °C for 24 hours after preparation, and were dried again in a vacuum oven at the same temperature for another 24 hours just before thermal analysis. The TGA curves show the same shape, which is an indication that their degradation process is similar. The percent residue obtained at temperature of 600 °C decreases systematically with the alkyl chain length in the exchanged LDHs – from 45% residue for MgAl–C10 to 29% for MgAl–C22. This is in very good agreement with the inorganic content in these materials (*cf.* Table 2), and simply denotes that all the alkyl carboxylate content thermally decomposes by 600 °C.

When these LDHs are used as fillers in PMMA nanocomposites, they are effective in improving the thermal stability of the polymer matrix. Specifically, Fig. 7 compares the TGA results for virgin (unfilled) PMMA and PMMA nanocomposites with MgAl–C18 The addition of the alkyl-exchanged MgAl–LDHs improves the thermal stability of PMMA for all filler loadings. The degradation of the PMMA and its nanocomposites proceeds in two steps, which is consistent with previous studies.[25] Moreover, TGA analyses of the PMMA nanocomposites with the rest of the alkyl-exchanged MgAl–LDHs yields similar results (see ESI†), indicating that the thermal degradation process of the composites is similar for all exchanged LDH fillers. The detailed results from the TGA studies are summarized in Table 3, for PMMA and all of its LDH nanocomposites, as well as its composites with commercial MDH and ATH minerals. For the LDH-based nanocomposites, the mid-point temperature, at 50% degradation, $T_{0.5}$, in all the formulations is enhanced in comparison with the virgin polymer. There is no significant difference between $T_{0.5}$ as the LDH loading increases from 3, 5 to 10 wt% and also $T_{0.5}$ is almost constant as the alkyl chain length increases. However, the % char for the PMMA nanocomposites increases with an increase in the MgAl–LDH loading. In fact, more char is produced than is expected based simply on the amount of added LDH; the increase in char may be the due to some condensed phase mechanism taking place during thermal degradation.

Table 3 Summary of TGA data for PMMA its alkyl carboxylate MgAl nanocomposites and its composites with MDH and/or ATM[a]

PMMA composites with alkyl carboxylate-exchanged MgAl LDH					
Formulation	$T_{0.1}$/°C	$T_{0.5}$/°C	% Residue	$\Delta T_{0.5}$	$\Delta T_{0.1}$
Pure (unfilled) PMMA	281	355	1	—	—
PMMA + 3% MgAl–C10	300	384	4	29	19
PMMA + 5% MgAl–C10	299	387	5	32	18
PMMA + 10% MgAl–C10	297	388	8	33	16
PMMA + 3% MgAl–C12	296	388	4	33	15
PMMA + 5% MgAl–C12	297	389	6	34	16
PMMA + 10% MgAl–C12	296	393	8	38	15
PMMA + 3% MgAl–C14	297	387	3	32	16
PMMA + 5% MgAl–C14	294	388	5	33	13
PMMA + 10% MgAl–C14	294	394	7	39	13
PMMA + 3% MgAl–C16	298	387	3	32	17
PMMA + 5% MgAl–C16	298	390	5	35	17
PMMA + 10% MgAl–C16	296	394	7	39	15
PMMA + 3% MgAl–C18	294	385	4	30	13
PMMA + 5% MgAl–C18	297	384	4	29	16
PMMA + 10%MgAl–C18	297	391	7	36	16
PMMA + 3% MgAl–C22	297	385	3	30	16
PMMA + 5% MgAl–C22	296	387	5	32	15
PMMA + 10% MgAl–C22	298	391	7	36	17
PMMA Composites with MDA, ATM and MDH/ATM mixtures					
Formulation	$T_{0.1}$/°C	$T_{0.5}$/°C	% Residue	% Residue expected	$\Delta T_{0.1}$
Pure (unfilled) PMMA	278	357	0	0	—
PMMA + 3% MH	290	384	5	2	12
PMMA + 5% MH	292	383	6	3	14
PMMA + 10% MH	299	386	9	7	21
PMMA + 20% MH	298	398	10	14	20
PMMA + 3% ATH	281	372	3	2	3
PMMA + 5% ATH	280	369	4	3	2
PMMA + 10% ATH	280	374	6	7	2
PMMA + 20% ATH	282	390	13	13	4
PMMA + 2.0% MH + 1.0% ATH	286	376	4	2	8
PMMA + 3.3% MH + 1.7% ATH	283	384	6	3	5
PMMA + 6.7% MH + 3.3% ATH	288	390	10	7	10

[a] $T_{0.1}$ = temperature at 10% mass loss; $T_{0.5}$ = temperature at 50% mass loss, % residue at 600 °C; $\Delta T_{0.5}$ and $\Delta T_{0.1}$ = difference of $T_{0.5}$ and $T_{0.1}$ between the nanocomposite and the matrix; % residue expected = based on the TGA curve of the minerals.

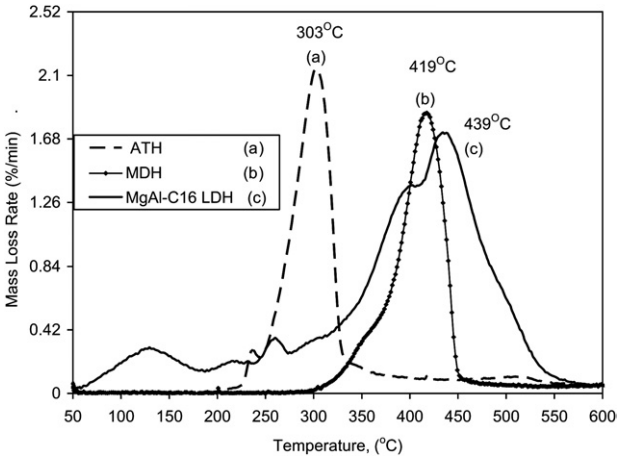

Fig. 8 DTG of additives (a) ATH, (b) MDH and (c) MgAl–C16 LDH.

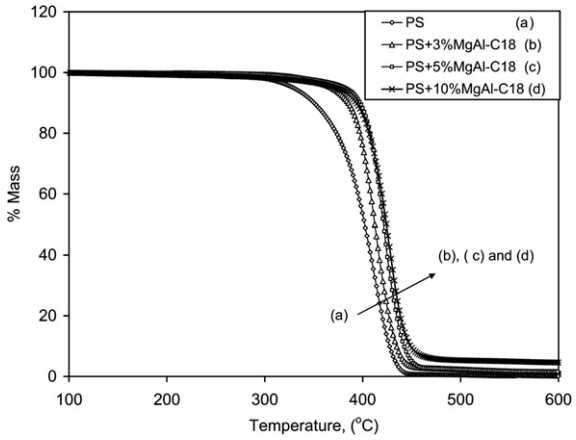

Fig. 9 TGA curves for bulk polymerized for (a) PS, (b) PS + 3% MgAl–C18, (c) PS + 5% MgAl–C18 and (d) PS + 10% MgAl–C18.

Table 4 Summary of TGA data for PS its alkyl carboxylate MgAl nanocomposites and its composites with MDH and/or ATM[a]

PS composites with alkyl carboxylate-exchanged MgAl LDH					
Formulation	$T_{0.1}$/°C	$T_{0.5}$/°C	% Residue	$\Delta T_{0.5}$	$\Delta T_{0.1}$
Pure (unfilled) PS	349	401	—	—	—
PS + 3% MgAl–C10	397	422	2	21	48
PS + 5% MgAl–C10	402	425	2	24	53
PS + 10% MgAl–C10	388	421	6	20	39
PS + 3% MgAl–C11	358	413	1	12	9
PS + 5% MgAl–C11	380	423	3	22	31
PS + 10% MgAl–C11	369	426	4	25	20
PS + 3% MgAl–C12	372	406	1	5	23
PS + 5% MgAl–C12	390	418	3	17	41
PS + 10% MgAl–C12	390	422	4	21	41
PS + 3% MgAl–C14	392	418	1	17	43
PS + 5% MgAl–C14	396	421	2	20	47
PS + 10% MgAl–C14	398	424	4	23	49
PS + 3% MgAl–C16	375	414	1	13	26
PS + 5% MgAl–C16	385	417	2	16	36
PS + 10% MgAl–C16	384	420	4	19	35
PS + 3% MgAl–C18	385	412	2	11	36
PS + 5% MgAl–C18	397	420	2	19	48
PS + 10% MgAl–C18	394	424	5	23	45
PS + 3% MgAl–C22	395	420	1	19	46
PS + 5% MgAl–C22	388	421	3	20	39
PS + 10% MgAl–C22	401	427	3	26	52
PS composites with MDH, ATH and MDH–ATH mixtures					
Formation	$T_{0.1}$/°C	$T_{0.5}$/°C	% Residue	% Residue expected	$\Delta T_{0.1}$
Pure (unfilled) PS	404	428	0	0	—
PS + 3% MH	398	432	2	2	−6
PS + 5% MH	396	429	3	3	−8
PS + 10% MH	403	438	7	7	−1
PS + 20% MH	399	439	14	14	−5
PS + 3% ATH	400	436	14	2	−5
PS + 5% ATH	406	442	4	3	2
PS + 10% ATH	404	446	7	7	0
PS + 20% ATH	403	451	15	13	−1
PS + 2.0% MH% + 1% ATH	404	432	2	1	0
PS + 3.3% MH% + 1.7% ATH	396	431	3	3	−8
PS + 6.7% MH% + 3.3% ATH	406	446	7	7	2

[a] $T_{0.1}$ = temperature at 10% mass loss; $T_{0.5}$ = temperature at 50% mass loss, % residue at 600 °C; $\Delta T_{0.5}$ and $\Delta T_{0.1}$ = difference of $T_{0.5}$ and $T_{0.1}$ between the nanocomposite and the matrix; % residue expected = based on the TGA curve of the minerals.

When comparing the PMMA–LDH nanocomposites to the composites based on MDH and ATH, the flame-retardancy effect of the LDH is similar, to some extent, to that of a mixture of MDH and ATH. In fact, Camino *et al.*[2] have shown that thermal behavior of MgAl–carbonate LDH is comparable to MDH and ATH in terms of heat absorption capacity and mass loss. A comparison between the exchanged LDH and the commercial minerals is shown in Fig. 8, by comparing their differential thermogravimetric (DTG) curves. Despite the differences in the DTG of the two classes of fillers, there is reasonable agreement in terms of $T_{0.1}$ and $T_{0.5}$ TGA temperatures between the two classes of composites (Table 3); *i.e.*, between the LDH-based PMMA nanocomposites and PMMA composites based on MDH, ATH, and mixtures of the two (all TGA curves are provided in the ESI†). It should be noted that the exchanged LDHs contain between 55 and 70% organic, which implies that the loading of the minerals is substantially larger than the inorganic content of the LDH nanocomposites. Nonetheless, there is a larger amount of char formed in the LDHs nanocomposites, substantially higher than the inorganic content in the respective nanocomposites, which suggests that the LDH most probably have an effect different from that of the MDH/ATH minerals, whose composites char yield follows rather well the inorganic content (Table 3).

Qualitatively similar trends are observed in the TGA studies of PS composites based on the same fillers. Fig. 9 shows the TGA curves of PS with MgAl–C18 and the detailed TGA data for all the composites is tabulated in Table 4. All the TGA curves for PS composites with alkyl-exchanged MgAl–LDHs are similar and are presented in the ESI†. In the case of the PS composites, the addition of the LDH enhances both $T_{0.1}$ and $T_{0.5}$, an effect which is not seen for the melt blended composites with MDH and/or ATH. For the onset temperature of the degradation, the typical enhancement in temperature upon addition of the LDH is about 40 degrees; whereas the mid-point of the degradation typically shows about a 20 degrees increase. The TGA data for the various composites of PS, with the MDH/ATH minerals and the LDHs, is tabulated in Table 4 and all of the curves are shown in the ESI†. There is a qualitative similarity between the TGA behavior of the composites based on the exchanged LDH and those based on the commercial minerals.

4. Fire retardancy of the PMMA/MgAl–LDHs composites

The cone calorimeter is the most effective method for the laboratory evaluation of the fire properties of polymers. The heat release rate, HRR, and in particular its peak value, PHRR, is one of the important parameters. Table 5 presents the cone calorimetry data obtained at a heat flux of 50 kW m^{-2} for the PMMA and its nanocomposites, and Table 6 summarizes the cone calorimetry results obtained at a heat flux of 35 kW M^{-2} for the bulk polymerized PS and its composites. The data shows that the PHRR is reduced with an increase in the MgAl–LDH loading. In each set of formulation, an increase in loading of MgAl–LDHs from 3 to 10% decreases the PHRR, average mass loss rate, total heat released and increases the smoke, as measured by ASEA. The heat release rate, particularly the PHRR, is reduced significantly at 10% loading of MgAl–LDH, for all the alkyl carboxylates used. This reduction may be attributed to the change in the mass loss rate and the increase in the MgAl–LDH content, which decomposes and releases water vapor, cooling the pyrolysis zone at the combustion surface. The most effective composite formulations for PS are those with MgAl–C10 and MgAl–C12; longer chain systems destabilize the polymer. For PMMA, there is much less dependence on the length of the carboxylate. This is clearly shown in the plot of PHRR *vs.* number of carbons in the LDH in Fig. 10. A similar effect is noted with PS systems in which the addition of MgAl–LDH significantly reduces the PHRR as the MgAl–LDH loading increases. The best PHRR reduction in PS is 56% observed at 10% loading with the MgAl–C10 followed by 52% from the MgAl–C12; the

Table 5 Cone calorimetry results for PMMA and its MgAl–LDHs nanocomposites (at 50 kW m^{-2})[a]

Formulation	PHRR/kW m^{-2}	Redct %	THR/MJ m^{-2}	ASEA/m^2 kg^{-1}	AMLR/g s^{-1} m^{-2}	t_{ig}/s
Pure PMMA	1043 ± 50	—	92 ± 2	122 ± 9	36 ± 1	20 ± 2
PMMA + 3% MgAl–C10	788 ± 63	24	64 ± 28	165 ± 12	25 ± 4	20 ± 1
PMMA + 5% MgAl–C10	631 ± 57	40	70 ± 31	248 ± 90	20 ± 1	16 ± 1
PMMA + 10% MgAl–C10	442 ± 22	58	85 ± 10	212 ± 46	19 ± 9	16 ± 2
PMMA + 3% MgAl–C12	665 ± 34	36	86 ± 1	161 ± 6	22 ± 1	17 ± 1
PMMA + 5% MgAl–C12	550 ± 19	47	84 ± 1	196 ± 11	18 ± 1	14 ± 4
PMMA + 10% MgAl–C12	448 ± 83	57	79 ± 2	284 ± 31	10 ± 2	14 ± 2
PMMA + 3% MgAl–C14	774 ± 14	26	82 ± 3	172 ± 7	23 ± 1	16 ± 4
PMMA + 5% MgAl–C14	635 ± 24	39	80 ± 2	202 ± 14	19 ± 1	17 ± 0
PMMA + 10% MgAl–C14	484 ± 37	54	74 ± 3	320 ± 20	9 ± 1	15 ± 2
PMMA + 3% MgAl–C16	746 ± 29	29	83 ± 2	182 ± 11	22 ± 1	19 ± 1
PMMA + 5% MgAl–C16	728 ± 30	30	81 ± 1	194 ± 17	21 ± 2	17 ± 3
PMMA + 10% MgAl–C16	485 ± 31	54	73 ± 5	328 ± 5	10 ± 2	19 ± 1
PMMA + 3% MgAl–C18	786 ± 32	25	85 ± 1	163 ± 6	24 ± 2	17 ± 0
PMMA + 5% MgAl–C18	699 ± 27	33	83 ± 2	185 ± 6	21 ± 1	15 ± 1
PMMA + 10% MgAl–C18	515 ± 15	51	78 ± 4	325 ± 9	11 ± 1	15 ± 2
PMMA + 3% MgAl–C22	847 ± 31	19	84 ± 3	160 ± 9	25 ± 1	18 ± 3
PMMA + 5% MgAl–C22	714 ± 45	32	87 ± 0	200 ± 2	20 ± 1	20 ± 1
PMMA + 10% MgAl–C22	534 ± 28	49	83 ± 1	284 ± 20	12 ± 1	13 ± 3

[a] PHRR, peak heat release rate; THR, total heat released; ASEA, average specific extinction area; t_{ig}, time to ignition.

Table 6 Cone calorimetry results for PS and its MgAl–LDHs nanocomposites (at 35 kW m^{-2})[a]

Formulation	PHRR/kW m^{-2}	Redct %	THR/MJ m^{-2}	ASEA/m^2 kg^{-1}	AMLR/g s^{-1} m^2	t_{ig}/s
PS	1116 ± 25	—	97 ± 5	1271 ± 35	27 ± 0	52 ± 2
PS + 3% MgAl–C10	778 ± 47	30	96 ± 1	1569 ± 76	21 ± 1	18 ± 4
PS + 5% MgAl–C10	678 ± 19	39	99 ± 4	1513 ± 290	17 ± 1	37 ± 2
PS + 10% MgAl–C10	491 ± 31	56	96 ± 17	1900 ± 567	12 ± 1	7 ± 1
PS + 3% MgAl–C11	1013 ± 48	9	100 ± 3	1217 ± 24	25 ± 2	32 ± 4
PS + 5% MgAl–C11	1048 ± 87	6	99 ± 3	1216 ± 18	25 ± 1	23 ± 4
PS + 10% MgAl–C11	716 ± 298	36	79 ± 36	1308 ± 173	23 ± 1	22 ± 5
PS + 3% MgAl–C12	831 ± 43	26	104 ± 1	1222 ± 12	20 ± 1	31 ± 6
PS + 5% MgAl–C12	704 ± 32	37	105 ± 1	1234 ± 17	18 ± 1	19 ± 1
PS + 10% MgAl–C12	540 ± 12	52	100 ± 3	1400 ± 168	13 ± 1	31 ± 3
PS + 3% MgAl–C14	781 ± 15	30	105 ± 1	1304 ± 92	20 ± 1	17 ± 2
PS + 5% MgAl–C14	726 ± 51	35	107 ± 2	1382 ± 111	18 ± 2	31 ± 4
PS + 10% MgAl–C14	591 ± 15	47	103 ± 1	1376 ± 45	14 ± 1	38 ± 3
PS + 3% MgAl–C16	805 ± 25	28	105 ± 4	1295 ± 1	20 ± 1	18 ± 4
PS + 5% MgAl–C16	749 ± 18	33	108 ± 2	1314 ± 30	18 ± 1	26 ± 4
PS + 10% MgAl–C16	736 ± 34	34	108 ± 9	1308 ± 9	17 ± 1	26 ± 8
PS + 3% MgAl–C18	921 ± 81	17	113 ± 2	1322 ± 24	20 ± 1	34 ± 2
PS + 5% MgAl–C18	885 ± 20	21	116 ± 3	1354 ± 14	20 ± 0	33 ± 3
PS + 10% MgAl–C18	908 ± 54	19	114 ± 1	1320 ± 7	21 ± 1	19 ± 6
PS + 3% MgAl–C22	1083 ± 87	3	118 ± 4	1404 ± 46	21 ± 1	32 ± 5
PS + 5% MgAl–C22	1001 ± 48	10	114 ± 2	1375 ± 17	20 ± 1	29 ± 3
PS + 10% MgAl–C22	883 ± 67	21	116 ± 5	1451 ± 40	20 ± 1	18 ± 4

[a] PHRR, peak heat release rate; THR, total heat released; ASEA, average specific extinction area; t_{ig}, time to ignition.

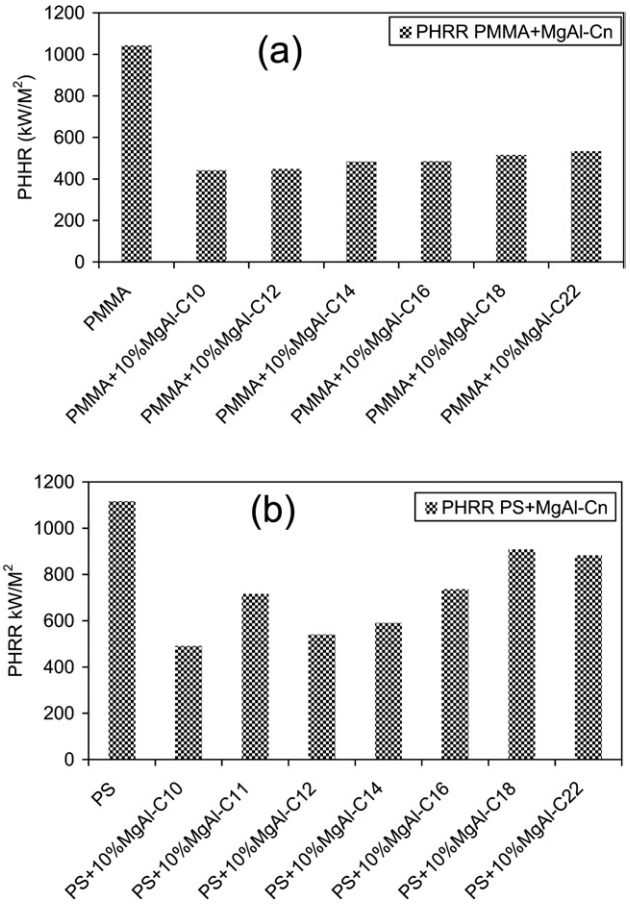

Fig. 10 PHRR plots for (a) PMMA + MgAl–C*n* LDHs and (b) PS + MgAl–C*n* LDHs.

lowest reduction is 21% from MgAl–C22. One might expect that as the organic content of the LDH increases, the fire load would also increase and there might be an increased PHRR, and this is observed. It is generally accepted that nanocomposites lead to good reductions in the PHRR, while montmorillonite microcomposites lead to essentially no reduction;[26] however, the C10- and C12-exchanged MgAl gave large PHRR reductions for the PS composites, comparable to those of well dispersed MMT nanocomposite,[27] despite the relatively poor filler dispersion. This suggests that dispersion does not play the same role in PS–LDH systems as it does in PS–MMT systems. For MMT, there is no effect on the PHRR unless there is also good nano-dispersion and this is obviously not the case with the LDHs. Work continues to identify the mechanism of action of the LDH family.

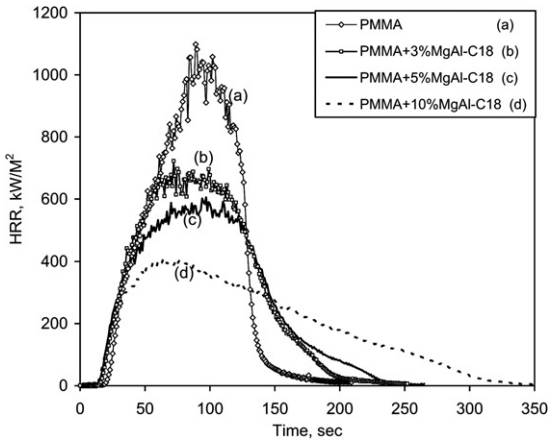

Fig. 11 HRR curves for PMMA/MgAl–C18 LDH at 50 kW m^{-2}.

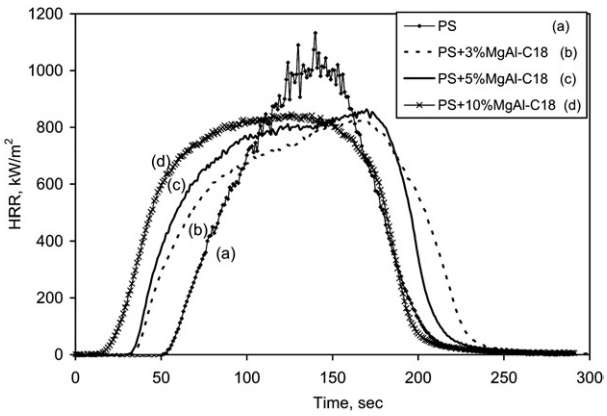

Fig. 12 HRR curves for PS/MgAl–C18 LDH at 35 kW m^{-2}.

The total heat is essentially unchanged, which is the normal observation for nanocomposites, simply indicating that the polymer eventually burns completely. The amount of smoke increases as the MgAl–LDH loading increases; the addition of an LDH leads to more smoke, perhaps connected in some way to the presence of the surfactant. The reduction in mass loss rate follows the reduction in PHRR, which is the typical observation for nanocomposites. The time to ignition for all the composites is shorter as compared to the virgin PS polymer, which is also the usual observation for clay composites.

The heat release rate curves for PMMA and PS with MgAl–LDHs are similar and are shown in the ESI†. Fig. 11 and Fig. 12 present representative heat release curves for PMMA and PS composites with exchanged MgAl LDHs, respectively. Two striking differences may be noted between the two polymers. For PMMA, the time to ignition does not change markedly upon nanocomposite formation, while there is a significant decrease for the PS composites; this has also been seen with montmorillonite (MMT) systems where PMMA does not show much change and almost all other polymers which have been investigated do change.[28] The second major difference is that PS systems show a much bigger spreading of the heat release rate curve than is seen for PMMA. This observation has not previously been made for MMT but this may be useful as information on how these systems work develops. Besides the reduction in PHHR, the cone calorimetry curves are also shifted towards a longer time of burning. The HRR curves are spread over a much longer period of time when the MgAl–LDH is used, especially at 10% loading. Since the TGA data show that char increases with MgAl–LDHs loading, the fire-retardant properties may also be due to the formation of char. This char insulates the burning material and reduces the amount of heat transferred to the polymer during combustion. The amount of char obtained in the cone calorimeter increases as the amount of LDH increases but it is still only a small fraction of the total mass. In previous work, it has been observed that the quality of the char is dependent upon the identity of the divalent metals that have been used. Here there is no difference in the type of char as the identity of the anion is changed. The fire-retardant character of the LDH composites can be attributed to the changes in the mass loss rate and the

Table 7 Cone calorimetry results for PS and PMMA composites with MDH and ATH[a]

Formulation	t_{ig}/s	PHRR/kW m^{-2}	Redct %	THR/MJ m^{-2}	AMLR/g s^{-1} m^{-2}	ASEA/m^2 kg^{-1}
PS	54 ± 2	1196 ± 46	—	100 ± 2	28 ± 9	1200 ± 249
PS + 3% MDH	46 ± 2	1110 ± 46	7	95 ± 1	25 ± 5	1143 ± 162
PS + 5% MDH	50 ± 3	1043 ± 30	13	95 ± 2	28 ± 2	1244 ± 42
PS + 10% MDH	48 ± 3	919 ± 27	23	94 ± 2	23 ± 5	1135 ± 176
PS + 20% MDH	47 ± 5	630 ± 15	47	84 ± 2	18 ± 2	1017 ± 220
PS + 3% ATH	35 ± 3	1152 ± 16	4	99 ± 1	25 ± 6	1328 ± 164
PS + 5% ATH	35 ± 4	1048 ± 38	8	101 ± 1	26 ± 1	1291 ± 36
PS + 10% ATH	31 ± 3	863 ± 37	28	96 ± 1	22 ± 1	1353 ± 83
PS + 20% ATH	33 ± 3	621 ± 3	48	80 ± 2	12 ± 1	1282 ± 366
PS + 2% MDH + 1% ATH	42 ± 2	1154 ± 41	4	101 ± 2	26 ± 2	1270 ± 18
PS + 3.3% MDH + 1.7% ATH	37 ± 2	1095 ± 47	8	101 ± 1	23 ± 7	1077 ± 166
PS + 6.7% MDH + 3.3% ATH	35 ± 1	889 ± 26	26	96 ± 1	23 ± 3	865 ± 162
PMMA	13 ± 3	933 ± 69	—	78 ± 2	13 ± 3	300 ± 17
PMMA + 3% MDH	13 ± 2	625 ± 26	33	72 ± 2	13 ± 2	191 ± 44
PMMA + 5% MDH	12 ± 4	544 ± 25	42	70 ± 1	12 ± 4	285 ± 85
PMMA + 10% MDH	13 ± 0	395 ± 10	58	64 ± 0	13 ± 0	235 ± 81
PMMA + 20% MDH	11 ± 1	316 ± 11	66	50 ± 1	11 ± 1	417 ± 90
PMMA + 3% ATH	9 ± 2	861 ± 19	8	73 ± 1	9 ± 2	604 ± 90
PMMA + 5% ATH	10 ± 2	853 ± 17	9	75 ± 0	10 ± 2	345 ± 56
PMMA + 10% ATH	10 ± 3	655 ± 24	30	70 ± 1	10 ± 3	107 ± 7
PMMA + 20% ATH	10 ± 3	341 ± 10	63	60 ± 2	10 ± 3	191 ± 30
PMMA + 2.0% MDH + 1.0% ATH	14 ± 7	684 ± 20	27	74 ± 3	14 ± 7	173 ± 27
PMMA + 3.3% MDH + 1.7% ATH	10 ± 1	599 ± 10	36	73 ± 3	10 ± 1	203 ± 39
PMMA + 6.7% MDH + 3.3% ATH	9 ± 2	445 ± 32	52	65 ± 2	9 ± 2	243 ± 46

[a] PHRR, Peak heat release rate; %Redct, % reduction compared to virgin PS or PMMA; THR, total heat released; t_{ig}, time to ignition; and ASEA, average specific extinction area. Cone calorimetry results for PS were obtained at heat flux of 35 kW m^{-2} and at 50 kW m^{-2} for PMMA.

decomposition of the LDHs, releasing water and thus diluting and cooling the pyrolysis zone.

Table 7 summarizes the cone calorimetry results for PS and PMMA composites with ATH, MDH and combinations of these fillers. The PHRR is reduced significantly with an increase in the loadings of MDH and ATH for both PS and PMMA. This reduction in PHRR is due to the endothermic decomposition of the MDH and ATH, which also release water that dilutes and cools the gases in the flame.[29] Combinations of 2 : 1 MDH to ATH showed improved fire performance in PMMA, compared to the use of ATH alone. This fire performance may be attributed to the additive effect of the fillers and is also comparable to that observed when MgAl–LDH is used in these polymers as presented in Table 5 and Table 6.

In PMMA, the presence of the nano-dispersed LDH at 10% loading gives essentially the same reduction in PHRR as the 10% loading of the MDH/ATH combination. Apparently the LDH is no more effective than the minerals. For PS, the situation is quite different. The LDH, which is not dispersed at the nano-level, is significantly better than the same combination of minerals. This is another indication of the complexity of the LDH systems as putative fire-retardant additives, and this topic is under active investigation.

4.7 Mechanical properties

The mechanical properties of the PS and PMMA composites are shown in Table 8. It must be emphasized that the values reported in this work are obtained for the polymers and nanocomposites without any processing aids or other additives; the pure unadulterated polymer was used. For both PS and PMMA composites the tensile strength was significantly reduced by the addition of the MgAl–LDHs, while the elongation at break remained unchanged. Previous literature[30,31] shows an increase in the tensile strength at low loadings of 1, 2, 3 and 4% loadings of LDH in polyimide and bulk polymerized PMMA. For loadings higher than 5%, it was observed that the tensile strength and elongation at break decreased significantly, albeit being higher than that of the respective virgin polymer. As presented in Table 8, the addition of high loadings of 10% MgAl–LDH in PS and PMMA compromises the tensile strength. This may be because some of the MgAl–LDH aggregates can act as stress concentration defects in both PS and PMMA composites as observed in the low magnification TEM images. No significant difference in the decrease of tensile strength and maximum elongation was observed when comparing across different alkyl carboxylate anions in the MgAl–LDH. It is well-known that the presence of nano-dispersed MMT in a polymer almost invariably leads to enhanced mechanical properties. From the TEM images one can see that the length of the LDH is smaller than that of a typical MMT and this decreased aspect ratio may be the reason that the mechanical properties are not enhanced here.

Table 8 Mechanical properties of the PMMA and PS, and their wt% MgAl LDH composites

Formulation	Tensile strength/MPa	Elongation at break (%)
PMMA	28 ± 5	5 ± 1
PMMA + 10% MgAl–C10	11 ± 1	5 ± 1
PMMA + 10% MgAl–C12	12 ± 5	5 ± 1
PMMA + 10% MgAl–C14	11 ± 1	5 ± 1
PMMA + 10% MgAl–C16	19 ± 3	3 ± 1
PMMA + 10% MgAl–C18	18 ± 5	3 ± 2
PMMA + 10% MgAl–C22	11 ± 2	2 ± 1
PS	17 ± 2	2 ± 1
PS + 10% MgAl–C10	10 ± 2	3 ± 1
PS + 10% MgAl–C11	12 ± 4	2 ± 1
PS + 10% MgAl–C12	9 ± 3	2 ± 2
PS + 10% MgAl–C14	15 ± 5	2 ± 0
PS + 10% MgAl–C16	11 ± 1	2 ± 1
PS + 10% MgAl–C18	12 ± 5	2 ± 1
PS + 10% MgAl–C22	11 ± 3	2 ± 1

4.8 Conclusions

MgAl–LDHs organically modified with a variety of alkyl carboxylate anions were prepared *via* exchange of a MgAl–nitrate LDH. Increases in *d*-spacing were observed by X-ray diffraction, indicating the presence of these carboxylate anions in the LDH interlayer. The corresponding TGA of the exchanged MgAl–LDH showed a decrease in the inorganic content (as indicated by the decrease in char) with an increase in the chain length of the carboxylate anions. PMMA and PS composites were prepared with the these MgAl–LDHs *via* melt blending and bulk polymerization, respectively. The TGA of these composites showed enhanced thermal stability and, more importantly, improved fire properties with good PHRR reduction at a 10 wt% MgAl–LDHs loading. The fire-retardant mechanism of MgAl–LDHs involves both changes in the mass loss rate and some cooling due to the release of water, and this mechanism is different from that of montmorillonite-based nanocomposites. For the polystyrene composites, poorly-dispersed LDHs (microcomposites) gave significant reductions in PHRR, comparable to the best reductions reported for well-dispersed montmorillonite fillers, indicating a significant difference in behavior for MMT and LDH. For PMMA, similar cone calorimetry results were obtained for composites with LDH and with a mixture of MDH and ATH at similar loading. In PS, the LDH, even though it is not dispersed at the nanometre level, gives enhanced fire properties compared to the same mixture of minerals. It is becoming increasingly clear that LDHs perform as fire-retardant additives by mechanisms that are quite different from those of montmorillonite clays.

Acknowledgements

The authors would like to thank Dr Sergey Lindeman for performing the powder X-ray diffraction analysis, Dr Jeanne Hossenlopp for helpful discussions and Dr Raymond Fournelle for access to mechanical testing facilities. Partial support for this work by the US Department of Commerce, National Institute of Standards and Technologies, Grant 60NANB6D6018 is gratefully acknowledged. The work at Penn State was supported through a grant by the Penn State University Agricultural Experiment Station, and access to the electron microscopy facilities of the Huck Institute for the Life Sciences is gratefully acknowledged.

References

1 (*a*) D. G. Evans and X. Duan, *Chem. Commun.*, 2006, **5**, 485; (*b*) S. Ling, D. Li, J. Li, D. Wang, D. G. Evans and X. Duan, *Chin. Sci. Bull.*, 2005, **50**, 1101; (*c*) G. Costantino, A. Gallipoli, M. Nocchetti, G. Camino, F. Belluci and A. Frache, *Polym. Degrad. Stab.*, 2005, **90**, 586.

2 G. Camino, A. Maffezzoli, M. Braglia, M. De Lazzaro and M. Zammarano, *Polym. Degrad. Stab.*, 2001, **74**, 457.

3 *Supermolecular organization and materials design*, ed. W. Jones and C. N. R Rao, Cambridge University Press, Cambridge, 2002; *Handbook of Layered Materials*, ed., S. M. Auerbach, K. A. Carrado and P. K. Dutta, Marcel Dekker, New York, 2004.

4 *Layered Double Hydroxides: Present and Future*, ed. V. Rives, Nova Science Publishers, Inc., New York, 2001.

5 V. R. L. Constantino and T. J. Pinnavaia, *Inorg. Chem.*, 1995, **34**, 883; S. Miyata, *Clays Clay Miner.*, 1975, **23**, 369.

6 M. A. Drezdzon, *Inorg. Chem.*, 1988, **27**, 4628.

7 H. P. Boehm, J. Steinle and C. Vieweger, *Angew. Chem., Int. Ed. Engl.*, 1977, **89**, 259.

8 D. J. Wang, G. Serrette, Y. Tian and A. Clearfield, *Appl. Clay Sci.*, 1995, **10**, 103.

9 C. Nyambo, D. Wang, C. A. Wilkie, *Polym. Adv. Technol.*, accepted for publication.

10 C. Manzi-Nshuti, D. Wang, J. M. Hossenlopp and C. A. Wilkie, *J. Mater. Chem.*, 2008, **18**, 3091.

11 M. Meyn, K. Benecke and G. Lagally, *Inorg. Chem.*, 1990, **29**, 5201.

12 G. A. Wang, C. C. Wang and Y. C. Chen, *Polymer*, 2005, **46**, 5065.

13 D. Wang, J. Zhu, Q. Yao and C. A. Wilkie, *Chem. Mater.*, 2002, **14**, 3837.

14 T. Lan, P. D. Kaviratna and J. T. Pinnavaia, *Chem. Mater.*, 1995, **7**, 2144.

15 M. Zammarano, S. Bellayer, J. W. Gilman, F. Massimiliano, F. L. Beyer, R. H. Harris and S. Meriani, *Polymer*, 2006, **47**, 652.

16 P. S. Newman and W. Jones, *New J. Chem.*, 1998, 105; W. T. Reichle, *J. Catal.*, 1985, **94**, 547.

17 K. Chibwe and W. Jones, *J. Chem. Soc., Chem. Commun.*, 1989, **14**, 926.

18 (*a*) E. Hackett, E. Manias and E. P. Giannelis, *J. Chem. Phys.*, 1998, **108**, 7410; (*b*) J. Zhang, E. Manias and C. A. Wilkie, *J. Nanosci. Nanotechnol.*, 2008, **8**, 1597.

19 S. Miyata and T. Kumura, *Chem. Lett.*, 1973, **8**, 843.

20 (*a*) V. Kuppa, S. Menakanit, R. Krishnamoorti and E. Manias, *J. Polym. Sci., Part B: Polym. Phys.*, 2003, **41**, 3285; (*b*) E. Manias, V. Kuppa, D. B. Zax and D.-K. Yang, *Colloids Surf., A*, 2001, **187–188**, 509.

21 (*a*) Z. M. Wang, T. C. Chung, J. W. Gilman and E. Manias, *J. Polym. Sci., Part B: Polym. Phys.*, 2003, **41**, 3173; (*b*) E. Manias, H. Chen, R. Krishnamoorti, J. Genzer, E. J. Kramer and E. P. Giannelis, *Macromolecules*, 2000, **33**, 7955; (*c*) R. A. Vaia, K. D. Jandt, E. J. Kramer and E. P. Giannelis, *Chem. Mater.*, 1996, **8**, 2628.

22 (*a*) M. C. Costache, M. J. Heidecker, E. Manias, R. K. Gupta and C. A. Wilkie, *Polym. Degrad. Stabil.*, 2007, **92**, 1753; (*b*) M. C. Costache, M. J. Heidecker, E. Manias, G. Camino, A. Frache, G. Beyer, R. K. Gupta and C. A. Wilkie, *Polymer*, 2007, **48**, 6532.

23 E. Manias and V. Kuppa, *Eur. Phys. J. E*, 2002, **8**, 193.

24 S. Su and C. A. Wilkie, *J. Polym. Sci., Part A: Polym. Chem.*, 2003, **41**, 1124.

25 M. C. Costache, D. Wang, J. M. Heidecker, E. Manias and C. A. Wilkie, *Polym. Adv. Technol.*, 2006, **17**, 272.

26 (*a*) M. Zanetti, G. Camino, D. Canavese, A. Morgan, F. Lamelas and C. A. Wilkie, *Chem. Mater.*, 2002, **14**, 189; (*b*) J. W. Gilman, C. L. Jackson, A. B. Morgan, R. Harris, Jr, E. Manias, E. P. Giannelis, M. Wuthenow, D. Hilton and S. H. Phillips, *Chem. Mater.*, 2000, **12**, 1866.

27 (*a*) J. Zhu, F. M. Uhl, A. B. Morgan and C. A. Wilkie, *Chem. Mater.*, 2001, **13**, 4649; (*b*) G. Chigwada, P. Jash, D. Jiang and C. A. Wilkie, *Polym. Degrad. Stab.*, 2005, **88**, 382.

28 P. Jash and C. A. Wilkie, *Polym. Degrad. Stab.*, 2005, **88**, 401.

29 W. E. Horn, "Inorganic Hydroxides and Hydroxycarbonates: Their Function and use as Flame-Retardant additives", in *Fire Retadancy of Polymeric Materials*, ed. A. F. Grand and C. A. Wilkie, Marcel Dekker, New York, 2000, p. 299.

30 H. B. Hsueh and C. Y. Chen, *Polymer*, 2003, **44**, 1151.

31 G. A. Wang, C. C. Wang and C. Y. Chen, *Polym. Degrad. Stab.*, 2006, **91**, 2443.

